Evidence for Strong Electronic Correlations in the Spectra of Gate-Doped Single-Wall Carbon Nanotubes

Holger Hartleb,[†] Florian Späth,[†] and Tobias Hertel[*,†,‡]

[†]Institute of Physical and Theoretical Chemistry, Faculty of Chemistry and Pharmacy, and [‡]Röntgen Research Center for Complex Material Systems, Julius-Maximilian University Würzburg, Am Hubland, 97074 Würzburg, Germany

ABSTRACT We have investigated the photophysical properties of electrochemically gate-doped semiconducting single-wall carbon nanotubes (s-SWNTs). A comparison of photoluminescence (PL) and simultaneously recorded absorption spectra reveals that free-carrier densities correlate well with the first sub-band exciton or trion oscillator strengths but not with PL intensities. We thus used a global analysis of the first sub-band exciton absorption for a detailed investigation of gate-doping, here of the (6,5) SWNT valence band. Our data are consistent with a doping-induced valence band shift according to $\Delta\epsilon_v = n \times b$, where n is the free-carrier density, ϵ_v is the valence band edge, and $b = 0.15 \pm 0.05$ eV·nm. We also predict such band gap renormalization of one-dimensional gate-doped semiconductors to be accompanied by a stepwise increase of the carrier density by $\Delta n = (32 m_{eff} b)/(\pi\hbar)^2$ (m_{eff} is effective carrier mass). Moreover, we show that the width of the spectroelectrochemical window of the first sub-band exciton of 1.55 ± 0.05 eV corresponds to the fundamental band gap of the undoped (6,5) SWNTs in our samples and not to the renormalized band gap of the doped system. These observations as well as a previously unidentified absorption band emerging at high doping levels in the Pauli-blocked region of the single-particle Hartree band structure provide clear evidence for strong electronic correlations in the optical spectra of SWNTs.

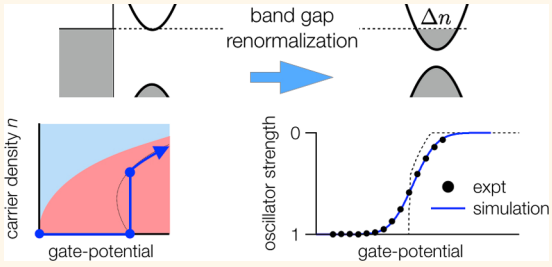

KEYWORDS: carbon nanotubes · gate doping · exciton photophysics · band gap renormalization · electronic correlation · trions

Electronic correlation is essential for an accurate description of the properties of atomic, molecular, and condensed matter,[1] but its importance for the photophysics of one-dimensional (1D) nanosystems is often far from well-understood. Strongly bound trion and exciton states capturing much of the oscillator strength of interband transitions in semiconducting single-wall carbon nanotubes (s-SWNTs)[2−6] suggest the presence of strong electronic correlations. Due to the intimate relationship of electronic screening and free-carrier densities, such correlations are expected to depend strongly on the free-carrier density n.[7] However, experimental evidence for the dependence of oscillator strengths, transition energies, or the emergence of new absorption bands on the density of free charge carriers in 1D systems is scarce.

Dimensionality and free charge carriers are known to be key factors in determining screening and for the ability of Coulomb interactions to introduce electronic correlations.[1] Excitonic states in semiconductors thus strongly depend on the dimension of a system, with binding energies in 3D semiconductors on the order of a few to tens of millielectronvolts but reaching up to 1 eV in the case of 1D s-SWNTs.[5] In spite of the importance of doping for transport, electron−hole correlations, screening,[7] trion binding,[8,9] electrochemistry,[10−12] or for the interpretation of spectroelectrochemical data from s-SWNTs,[13−28] charge-induced band gap renormalization (BGR)[6,29] and the associated redistribution of oscillator strengths in SWNTs have not yet been quantified experimentally. Here, we will address some of these issues by an investigation of the photophysics of electrochemically gate-doped s-SWNTs.

Initial spectroelectrochemical investigations of SWNTs were mostly carried out using vis−NIR absorption and Raman spectroscopy and revealed that signals from both types of spectroscopic probes could be reversibly bleached by electrochemical

* Address correspondence to tobias.hertel@uni-wuerzburg.de.

Received for review July 29, 2015 and accepted September 18, 2015.

Published online September 18, 2015
10.1021/acsnano.5b04707

© 2015 American Chemical Society

gate doping.[14,15,17,19,21,22,24] Changes in the Raman signals from the radial breathing mode of (6,5) SWNTs, for example, were initially attributed to a doping-induced bleach of transitions between higher sub-bands which were in resonance with the Raman laser line.[15] However, Kalbac *et al.*[14,19] and Dragin *et al.*[24] reported that higher-lying electronic transitions could already be modified at doping levels consistent with the filling of lower sub-bands. Dragin *et al.* thus speculated that doping might affect fundamental as well as secondary band gaps and the oscillator strengths of the associated (excitonic) transitions.[24]

However, no attempt toward a determination of fundamental band gaps from spectroelectrochemical absorption data was made until Paolucci *et al.* used a Nernstian analysis of changes in absorption signals from first sub-band exciton transitions to determine SWNT reduction and oxidation potentials from which they then calculated fundamental band gaps for a range of small-diameter SWNT types.[11,16] Interestingly, investigations using Nernsitan analysis of PL spectra appear to systematically yield smaller fundamental band gaps.[20,23] These discrepancies were tentatively attributed to environmental or solvent effects but appear to not have been fully resolved.

In this report, we will address some of the elementary questions which persist in the field, such as the justification for using a specific spectroscopic probe for the determination of fundamental band gaps and, in particular, the effect which electronic correlations and BGR are expected to have on such measurements. The paper is structured into five sections. In the first one, we present a comparison of different optical probes and spectral signatures for an assessment of fundamental band gaps. We show that PL signals depend nonlinearly on the doping level, and that gate doping of SWNTs is thus ideally probed using the first sub-band exciton oscillator strength. We next discuss how changes of exciton or trion oscillator strengths can be obtained from absorption spectra using a global analysis. In the third section, we develop a simple model to better understand the effect of BGR on optical spectra of one-dimensional gate-doped semiconductors. In turn, we also discuss how this can be used for an experimental determination of the degree of BGR in SWNTs. We then use these insights for a detailed analysis of the spectroelectrochemical window in SWNTs in light of predicted but experimentally unconfirmed BGR.[6] Lastly, we discuss additional evidence for strong electronic correlations using absorption spectra of heavily doped semiconducting SWNTs. Such evidence is provided by a previously unidentified, very broad absorption band in the Pauli-blocked region of the single-particle Hartree band structure. This band is referred to as *H*-band, in reference to the high doping levels at which it emerges.

RESULTS AND DISCUSSION

In the experiments described in the following, semiconducting single-wall carbon nanotubes (s-SWNTs) of the (6,5) type were doped electrochemically by applying a potential between a working electrode (WE), with which SWNTs are in contact, and a quasi-reference electrode (QRE) (Figure 1a). The capacitive coupling of s-SWNTs to the working electrode and to the electrolyte in Figure 1b is estimated to be on the order of a few hundred aF·μm^{-1} and 10 fF·μm^{-1}, respectively.[11,30] The gate potential thus essentially drops at the SWNT−WE interface (see Figure 1c).

Absorption and PL Spectra of Electrochemically Gate-Doped SWNTs. Figure 2a shows that changes of absorption spectra with gate potential are symmetric around the midgap charge neutrality point at -4.46 ± 0.10 V with respect to the vacuum level, in agreement with earlier spectroelectrochemical measurements.[16] At charge neutrality near the midgap, spectra are dominated by the first sub-band S_1 and second sub-band S_2 exciton transitions at 996 and 574 nm, respectively. The remaining features are associated with absorption by the (9,1) minority species at 931 nm, with phonon sidebands,[31,32] and below 378 nm with the wrapping poly[(9,9-dioctylfluorenyl-2,7-diyl)-*co*-bipyridine] (PFO−BPy) polymer.[33] At potentials above about 0.4 V and below −0.8 V with respect to the QRE, we observe the appearance of a feature at 1168 nm, which is commonly associated with the charged exciton or trion transition ($X^{\pm}$).[8,9] The dependence of the optical density (OD) of the excitons at 996 and 574 nm in Figure 2b as well as of the trion at 1168 nm on electrochemical

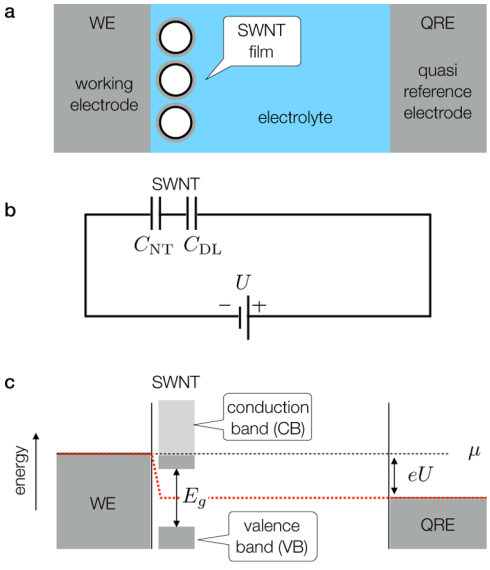

Figure 1. Schematic illustration of experimental setup for electrochemical gate doping. (a) Semiconducting SWNTs in contact with the working and quasi-reference electrode. (b) Equivalent circuit diagram with nanotube and double-layer capacitances. (c) Schematic energy diagram, illustrating that the gate potential drops at the nanotube−electrolyte interface because of its small double-layer capacitance.

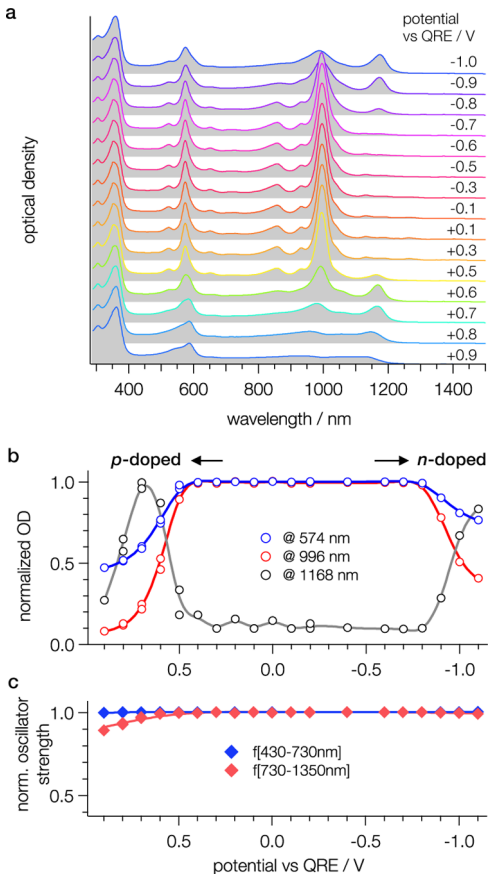

Figure 2. Spectra of gate-doped s-SWNTs. (a) Waterfall plot of UV−vis−NIR spectra of SWNTs doped by electrochemical gating. The first sub-band S_1 exciton at 996 nm is bleached at higher and lower potentials, while a trion feature $X^{\pm}$ develops at 1168 nm. At the highest doping levels, one also observes the emergence of a 0.9 eV wide, practically featureless absorption background between 630 and 1170 nm (see bottom spectrum at +0.9 V). (b) Optical densities of features in the vis and NIR spectral ranges change significantly, and (c) total oscillator strengths obtained from integrated spectra remain practically constant.

potential reveals a strong redistribution of oscillator strength at the highest and lowest potentials. However, integration of spectra over the NIR range from 730 to 1350 nm and over the vis range from 430 to 730 nm shows that the total oscillator strength is essentially conserved except for small changes at the highest positive potentials (blue and red diamonds in Figure 2c).

Integrated oscillator strengths thus remain practically constant even outside of the spectroelectrochemical window of the S_1 transition, which extends from about −1.0 V to +0.6 V (see Figure 2c). This suggests that any loss of S_1 oscillator strength is compensated by an increase of $X^{\pm}$ trion oscillator strength, at least up to the peak of the trion OD curves in Figure 2b. This is key for justifying the use of S_1 exciton absorption signals as a measure of free-carrier densities in SWNTs because an increase in trion (charged exciton) oscillator strength $f_{X^{\pm}}$ is identified with a concomitant increase of the doping level n. For the following detailed analysis of optical spectra near the drop-off of exciton signals at −1.0 V and +0.6 V, we will thus assume that the total oscillator strengths of trion and exciton $f_{S_1} + f_{X^{\pm}}$ are conserved. Consequently, the S_1 exciton oscillator strength f_{S_1} can be used as a direct measure of the doping level, with $f_{S_1} \propto (1 - n/n_b)$, where n_b signifies the charge density at which the S_1 exciton transition is completely bleached. We use $n_b = e/r_{e-h} = 0.5\ e \cdot nm^{-1}$ that corresponds to one charge per electron−hole correlation length (*i.e.*, "size") of the exciton with r_{e-h} = 2.0 nm, which was determined experimentally for (6,5) SWNTs.[34]

Before continuing with a discussion of PL signals, we point out that the asymmetry of the spectroelectrochemical window of the S_1 exciton OD in Figure 2b, specifically in the form of a slightly smaller slope in the drop-off toward negative potentials (n-doping), may be taken as evidence for a lower density of states (DOS) in the conduction band if compared with the valence band. This is in agreement with expectations based on the previously reported electron−hole band asymmetry for graphene and SWNTs, which implies that electron effective masses are somewhat lower than hole masses.[35]

Alternatively, gate doping of SWNTs has frequently also been studied using photoluminescence spectroscopy, in some instances with the aim of determining SWNT fundamental band gaps. However, as mentioned in the introduction, spectroelectrochemical windows determined from PL spectra systematically yield fundamental band gaps lower than those obtained from absorption or Raman spectra. To better understand this discrepancy, we have used a custom-built setup that simultaneously records PL and absorption spectra of gate-doped s-SWNTs from the NIR to the vis spectral range.

A series of simultaneously recorded PL and absorption spectra are shown in Figure 3a,b for the spectral range of the first sub-band exciton transition of (6,5) SWNTs, recorded at 25 mV increments for positive gate potentials between +0.200 and +0.700 V with respect to the Pt QRE. Optical densities at the first and second sub-band exciton transitions (open red and blue circles) and the PL intensity of the S_1 exciton (solid black circles) are compared in Figure 3c. The data show that the PL intensity drops off at significantly smaller potentials than the OD of the first or second sub-band excitons. In Figure 3d, we have plotted the PL quantum yield (solid black circles) as well as the OD of the second sub-band exciton (open blue circles) *versus* the S_1 oscillator strength (see discussion below). The latter is assumed to scale linearly with the doping level, which was added as the top axis to Figure 3d. It is evident that the aforementioned discrepancies between fundamental band gaps determined from PL and from absorption spectroscopy may be attributed to this strongly nonlinear dependence of the PL quantum

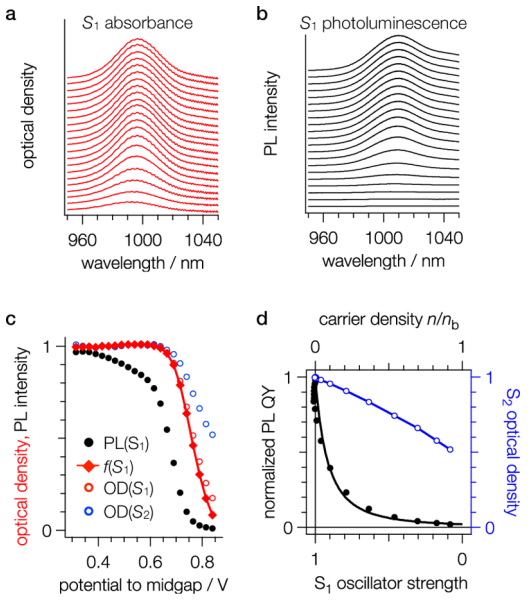

Figure 3. Dependence of different optical signatures on gate potential. Waterfall plots of (a) NIR absorption and (b) PL spectra of gate-doped (6,5) SWNTs recorded for positive potentials at 25 mV increments (from top to bottom). (c) Dependence of PL intensity (solid black circles), OD at first and second sub-band exciton wavelengths (open red and blue circles), and first sub-band exciton oscillator strength as determined from a global analysis (red diamonds). (d) Correlation of the normalized PL quantum yield from the S_1 exciton and the OD of the S_2 transition, where the S_1 oscillator strength clearly shows that neither the PL signal nor the S_2 OD exhibits a 1:1 correspondence with free-carrier densities.

yield on free-carrier densities. This is in agreement with the extraordinary susceptibility of SWNT excitons to nonradiative decay[36] and its nonlinear dependence on quenching site concentrations.[37] Such high sensitivity has been attributed to large exciton diffusion lengths in SWNTs, on the order of tens to hundreds of nanometers.[36,37]

The weaker dependence of the second sub-band exciton OD on free-carrier density in Figure 3d also suggests that spectroelectrochemical analysis of Raman data, resonantly enhanced by interaction with one of the higher sub-band transitions, is likely to overestimate the fundamental band gaps. For the following investigation of the effects of electrochemical gate doping on optical spectra and for the determination of fundamental band gaps, we will therefore focus on the first sub-band exciton in the absorption spectra.

Determination of S_1 Exciton Oscillator Strengths from Absorption Spectra. In the previous section, we argued that the oscillator strength of the S_1 exciton should represent the most accurate probe of doping levels that are needed for the frequently used Nernstian analysis of redox potentials.[16,20,26,28] However, the key assertions implicit to previous Nernstian interpretations of spectroelectrochemical data were (i) that optical densities can be associated with concentrations and (ii) that spectral changes during an electrochemical transformation can be attributed to the direct conversion of one set of reagents into one set of products. Unfortunately, neither assumption seems fully justified. One of the spectroscopic signatures of direct chemical transformations are isosbestic points in absorption spectra. Absorption spectra from gate-doped s-SWNTs, however, do not exhibit such isosbestic points (see Figure 4), which indicates that the oxidation or reduction of s-SWNTs is not a one-step but rather a sequential process with no evidence as to the number or spectral character of the reaction intermediates. Unfortunately, this calls the use of any optical signature for a determination of concentration changes into question unless a more detailed analysis can validate such an approach. In the following, we will thus discuss how the first sub-band exciton oscillator strength can be obtained from absorption spectra of doped SWNTs using a global analysis.[38]

The global analysis reveals that the combination of only three independent spectral components with appropriate spectral weights allows an excellent description of the experimental data in Figure 4a,d. The three components and the dependence of their spectral weights on gate potential are shown in Figure 4b,c for the NIR spectral range as well as in Figure 4e,f for the vis spectral range. The first component corresponds to the spectrum of the undoped (6,5) s-SWNT (red spectrum Figure 4b,c). The second component with maximum amplitude at +0.85 V with respect to midgap corresponds to the moderately doped (6,5) s-SWNTs, as evidenced by the trion peak at 1168 nm.[8,9] An asymmetric feature at 972 nm (blue spectrum) is attributed to a simultaneous blue shift of the S_1 exciton by up to nearly 50 nm, in agreement with predictions by Spataru and Léonard.[6]

The third component, associated with the heavily doped SWNT, emerges at potentials above ≈0.80 V with respect to the midgap. Here, absorption between 630 and 1170 nm becomes nearly constant and featureless (yellow spectrum in Figure 4a). We refer to this band as "*H*-band" because of its emergence in the heavily doped regime. This is is noteworthy because the absorption signal lies in a spectral region where interband transitions should be Pauli-blocked up to nearly twice the gate potential of 1.09 eV corresponding to about 565 nm (see red arrows in Figure 5b). Even asymmetric band renormalization[6,39] would make valence-to-conduction band transitions in this wavelength range highly improbable. Surprisingly, the intensity of the *H*-band is large, as evidenced by the nearly unchanged oscillator strengths of the vis and NIR spectral ranges seen in Figure 3d. By comparison with the known oscillator strength of the S_1 exciton,[40] we obtain an absorption cross section for the *H*-band of 1.7×10^{-18} cm^2 per carbon atom, corresponding to about 30% of the absorption cross section per atom in graphene.[41]

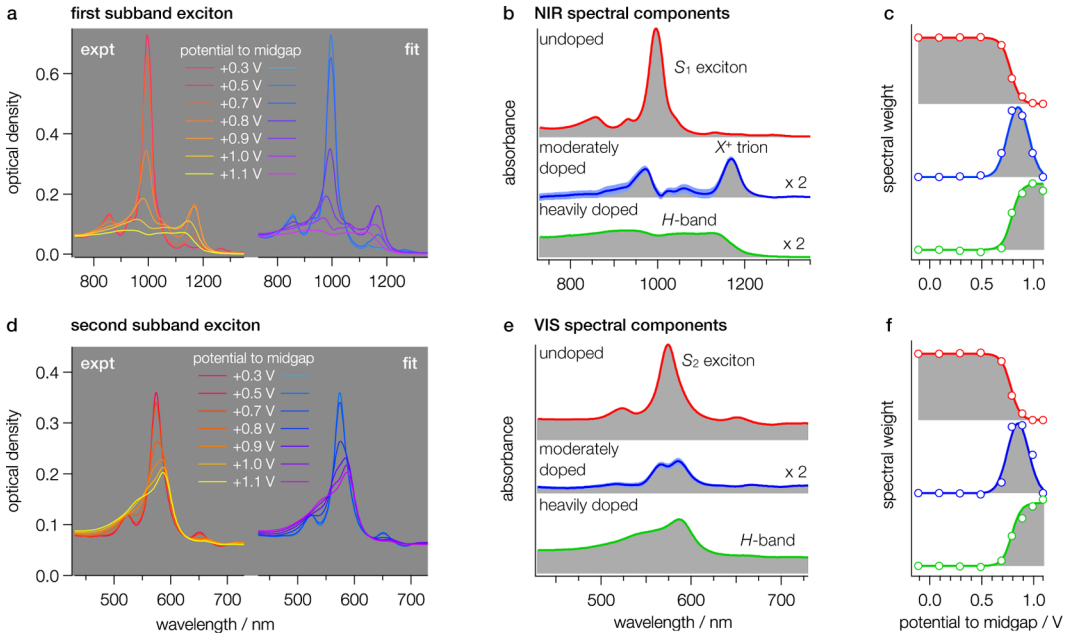

Figure 4. Analysis of absorption spectra at different doping levels. (a) NIR spectra at positive potentials (p-doping) and fit of data from a global analysis. (b) Optical spectra in (a) can be well described by the superposition of three spectral components, one for spectral signatures characteristic of the undoped, moderately doped, and heavily doped SWNTs. The blue confidence bands for the moderately doped component are rendered by the global fit. The first sub-band exciton at 996 nm is seen to disappear at potentials near 0.75 V, while a trion feature emerges at 1168 nm. The asymmetric feature in the moderately doped component at 972 nm is attributed to a blue shift of the exciton transition at moderate doping. (c) Potential dependence of the spectral weights of each of the three components. (d–f) Same as that in (a–c) but with data for the vis spectral range. Here, the second sub-band exciton merges into an asymmetric absorption band at higher free-carrier densities.

Role of BGR for the Interpretation of Spectroelectrochemical Data. Band gap renormalization has been predicted for SWNTs[6] and was suspected to be partly responsible for the unexpected bleach of Raman signals resonantly enhanced by higher sub-band transitions when only the lowest sub-bands were accessible to gate doping.[24] Since BGR is associated with a decrease of the fundamental band gap, we need to first investigate whether band gaps determined from the width of the S_1 spectroelectrochemical window correspond to the fundamental band gap of the undoped or to the reduced band gap of a the doped SWNT. In the latter case, the spectroelectrochemical window would provide only a lower bound of the actual fundamental band gap. Moreover, we need to understand if and how we may use the dependence of oscillator strengths on electrochemical potential for a determination of the extent of BGR.

To this end, we first discuss the anticipated effect of BGR on the electron or hole density, n, which can then be used for analysis of experimentally determined S_1 oscillator strengths. As illustrated schematically in Figure 5a–c, one of the crucial consequences of doping-induced BGR is that valence and conduction band edges are shifted, so as to draw additional charges into the semiconductor (Figure 5b,c). To better understand the implications of this positive feedback mechanism for the dependence of free-carrier densities on gate potential, we need to abandon the frequently used "rigid band" approximation.[21,22] We thus allow for BGR, which is parametrized within an effective medium approximation in terms of the free-carrier density n, as $\epsilon = \epsilon^{(0)} \pm bn$, with ϵ being the valence or conduction band edge and b being a parameter characteristic of the strength of BGR (the $\pm$ signs refer to shifts of valence or conduction bands, respectively). Free-carrier bands are represented within the effective mass approximation. The resulting dependence of n on the gate potential U and on band edge ϵ then becomes

$$n(U,\epsilon) = \frac{\sqrt{32 m_{\mathrm{eff}}}}{\pi\hbar}\,(|eU - \epsilon|)^{1/2} \qquad (1)$$

with e being the electron charge and m_{eff} being the valence or conduction band effective free-carrier mass (see Supporting Information, SI). This function is shown in Figure 5d as the curved red surface. The hypothetical couplings of free-carrier density and band edge for different values of b are illustrated as a fan of lines on the green n–ϵ plane in Figure 5d, with different slopes representing different strengths of BGR. Their projection onto the red $n(U,\epsilon)$ surface in Figure 5d yields the actual dependence of free-carrier density on the gate potential and on the band edge (or fundamental band gap). One of these parabolas is plotted in Figure 5e as a function of the gate potential U. In the presence of finite BGR and depending on the gate potential, this model thus supports one or three possible charge states

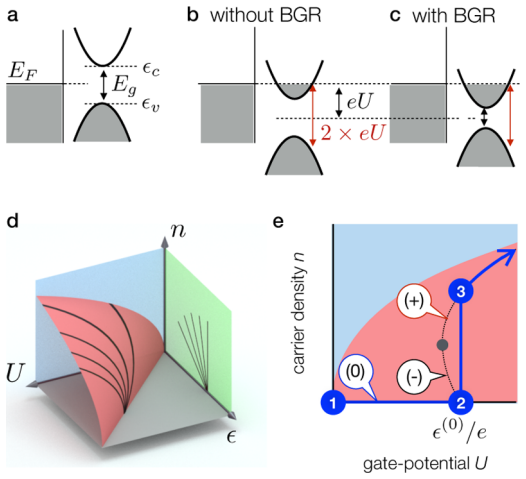

Figure 5. Influence of band gap renormalization on gate doping. (a−c) Schematic illustration of band alignment and band renormalization by electronic correlation when a semiconductor is gate-doped. The red arrows in (b) indicate the extent of the Pauli-blocked regime. (d) Dependence of free-carrier density on gate potential U and majority carrier band edge ϵ. Electronic correlations lead to a reduction of the gap at higher free-carrier densities. Different degrees of correlation are signified by the fan of lines in the green $n-\epsilon$ plane. One of their projections onto the red surface in the blue $n-U$ plane is shown in (e). As the potential is increased, the semiconductor remains uncharged up to point 2, at which the free-carrier density increases suddenly and the system transitions to point 3 from where it continues along the heavily doped (+) branch.

(see Figure 5e). They are designated as (0) undoped (blue line between points 1 and 2 in Figure 5e), (−) moderately doped, and (+) heavily doped (see SI).

For symmetric valence and conduction bands, we find that the undoped (0) branch is energetically favored up to the point where the gate potential reaches the band edge of the undoped system $\epsilon^{(0)}/e$ (see SI). Calculations by Spataru and Léonard[6] suggest that a reduction of the effective mass in the majority free-carrier band, combined with a stronger shift of the minority free-carrier band and the increase of its effective mass, may lead to additional stabilization of the undoped (0) branch up to $U = \epsilon^{(0)}/e$ beyond which point the system has no choice but to continue toward higher potentials along the heavily doped (+) branch. This suggests that gate doping of a 1D semiconductor in the presence of BGR leads to a sudden transition from undoped to more strongly doped when the gate potential reaches the band edge. Within the effective medium and effective mass approximations discussed above, the magnitude of the associated charge step is given by

$$\Delta n = \frac{32 m_{\text{eff}} b}{(\pi\hbar)^2} \qquad (2)$$

Consequently, the shift of the band edge becomes $32 m_{\text{eff}} b^2/\pi^2\hbar^2$.

In Figure 6, we contrast the qualitative charging behavior for gate doping of a 1D semiconductor with

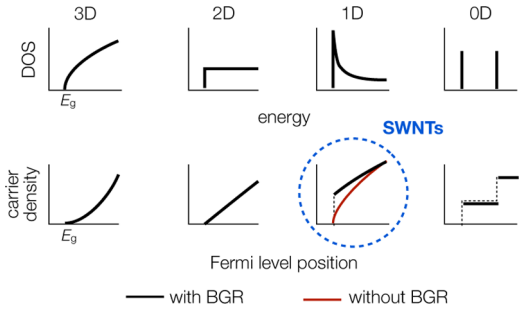

Figure 6. Dimensionality and doping-induced BGR. Schematic illustration of the DOS and resulting free-carrier density for gate-doped 3D, 2D, 1D, and 0D semiconductors. Band gap renormalization due to electronic correlations leads to a stepwise increase of the doping level in the case of 1D systems, in contrast to higher-dimensional systems.

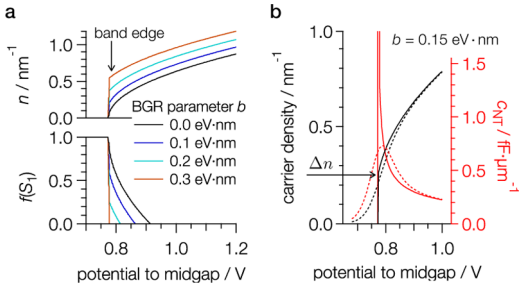

Figure 7. Dependence of oscillator strengths and doping level on BGR. (a) Free-carrier densities (top) and exciton oscillator strengths (bottom) as a function of gate potential for different BGR parameters. (b) Calculated free-carrier density and quantum capacitance for b = 0.15 eV·nm (solid lines), including thermal broadening (dashed lines).

the expected behavior for 3D, 2D, and 0D semiconductors. The 3D and 2D semiconductor densities of states are expected to support a continuous increase of the free-carrier density irrespective of the magnitude of possible BGR, while charging of a 1D semiconductor is fundamentally different due to the charge step at the band edge. As discussed briefly in the following, this unique behavior may be obscured by thermal excitations and by disorder.

In the top section of Figure 7a, we show the dependence of free-carrier density on the gate potential, as predicted by our model and as illustrated schematically by the blue line in Figure 5e. The curves represent the behavior for different values of the BGR parameter b, with the charge step Δn clearly increasing for larger values of b. The corresponding oscillator strengths in the lower part of Figure 7a are obtained from $f_{S_1} \propto (1 - n/n_b)$ as discussed earlier. It is evident that the slope of the f_{S_1} drop-off at the valence or conduction band edge can be steep or small depending on the strength of BGR. In the next section, we will use this observation for an assessment of the magnitude of BGR by comparison with the drop-off in our experimental data.

In Figure 7b, we plot the free-carrier density and the corresponding quantum capacitance c_{NT} for b = 0.15 eV·nm, calculated using $c_{NT} = e[\partial n(U)/\partial U]$.

To illustrate the effect of thermal broadening, we have also convoluted these curves with a Fermi function (dashed lines in Figure 7b). The discrete charge step at the band edge will thus enhance the capacitance expected for the van Hove type singularity of a rigid 1D band structure and may become accessible experimentally if the ratio k_BT/b and the inhomogeneous broadening of experimental data are sufficiently small.

Determination of the Degree of BGR from Experimental Oscillator Strengths. Next we focus on a discussion of how experimental data may provide evidence for BGR and how it allows one to quantitatively assess the BGR parameter b. To this end, we measured changes of the S_1 exciton absorption at the valence band edge of the spectroelectrochemical window using smaller gate potential increments (see Figure 8a). The f_{S_1} drop-off toward positive gate potentials has a slope of -6.5 ± 0.2 V^{-1} (see Figure 8a).

To compare this slope with predictions from our model, we calculated spectroelectrochemical windows of the S_1 oscillator strength for BGR parameters ranging from 0 to 0.5 V·nm (see Figure 8a). The calculated traces were convoluted with a room temperature Fermi distribution, including an additional inhomogeneous contribution of 42 mV, which was inferred from the spectral width of the S_1 exciton transition. The slope of the resulting drop-off in the calculated spectroelectrochemical windows is shown in Figure 8b as a function of the BGR parameter b (blue curve) along with the confidence range of the experimentally determined slope (red line and pink regions).

As seen from Figure 8b, we obtain best agreement between the slope of the experimental and the calculated signal drop-off using $b = 0.15 \pm 0.05$ eV·nm. Here, we used an effective mass of 0.07 m_e, as obtained from curvature-corrected tight-binding band structure calculations[42] and accounting for a 40% doping-induced reduction of the effective mass in majority free-carrier bands.[6,39] Within the above model, this suggests that the valence band edge is raised in energy by 40 meV, while the free-carrier density increases by 0.27 ± 0.10 nm^{-1} when the gate potential reaches the valence band edge of the undoped (6,5) SWNT. The resulting best fit to experimental data is shown in Figure 8a as a black dashed line (not broadened) and as a solid red line (broadened).

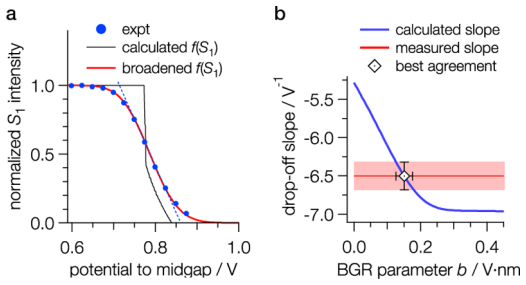

Figure 8. Determination of the BGR parameter b. (a) Experimental bleach of the first sub-band exciton (solid blue markers), slope at the inflection point (dashed blue line), and best fit of the calculated (black line) and broadened oscillator strengths (red line). (b) Comparison of experimentally determined slope in (a) (red line) with calculated slopes for different BGR parameters (blue line). The point of best agreement between experimental and calculated data is indicated by the black diamond at b = 0.15 eV·nm.

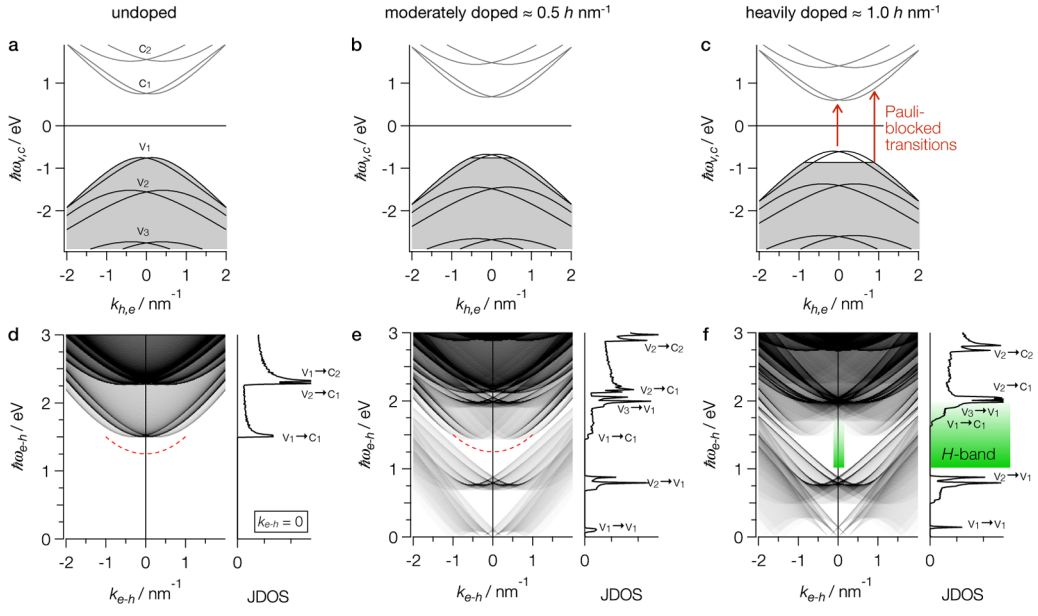

Figure 9. Single-particle bands and excitation spectra. (a–c) Tight-binding band structure of (6,5) SWNTs in the extended zone scheme for undoped, moderately doped, and heavily doped SWNTs. (d–f) Corresponding two-particle momentum-resolved excitation spectra as well as joint densities of states for $k_{e-h} = 0$. None of the features in the JDOS can be clearly attributed to the spectral signatures observed experimentally, underlining the importance of electronic correlations and many particle effects at all doping levels. The dashed red lines indicate the approximate location of the first sub-band exciton.

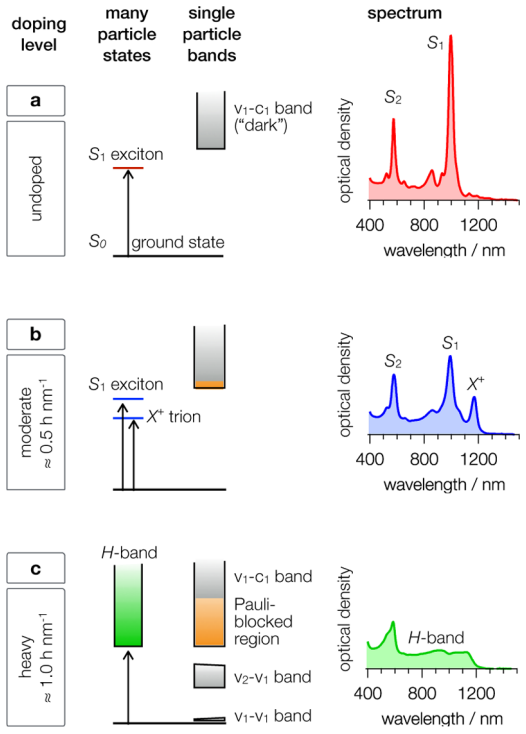

Figure 10. Signatures of electronic correlation in the spectra of s-SWNTs. (a–c) Schematic illustration of the energetics of many particle states observed experimentally and the single-particle bands predicted by a simple tight-binding calculation. None of the single-particle transitions can be observed experimentally, indicating the importance of electronic correlations and many-particle effects at all doping levels studied here.

Evidence for Strong Electronic Correlations in Spectra of Heavily Doped s-SWNTs. Lastly, we return to the unexpected 0.9 eV wide and featureless *H*-band observed in heavily doped s-SWNTs (Figure 2a and Figure 4). As mentioned earlier, its appearance is surprising because a single-particle band structure model cannot account for transitions in this energy range due to Pauli blocking of $v_1 \rightarrow c_2$ transitions. This is illustrated in Figure 9, where we have reproduced tight-binding band structure calculations of (6,5) SWNTs in the extended zone scheme, including the predicted band gap shifts induced by doping.[42] In Figure 9d–f, we show the corresponding momentum-resolved two-particle excitation spectra along with the respective joint densities of states (JDOS) and band assignments for specific transition regions.

As expected, the JDOS of the undoped (6,5) SWNT in the NIR and vis spectral range of Figure 9d is governed by valence-to-conduction band transitions $v_1 \rightarrow c_1$ as well as $v_1 \rightarrow c_2$ and $v_2 \rightarrow c_1$. New intra- and interband transitions emerge for moderate and heavy doping but do not lend themselves to an interpretation of transitions in the *H*-band between 1.05 and 1.95 eV (see green shaded area in Figure 9f). Curiously, we find that the Pauli-blocked transitions between the first valence and first conduction band of the renormalized band structure would coincide nicely with the energy range of *H*-band transitions.

We summarize the findings of the last section in Figure 10, where we show schematic energy level diagrams for experimentally observed many particle states as well as the corresponding single bands for undoped, moderately doped, and heavily doped SWNTs. The poor correlation of the single-particle structures with the experimentally observed first sub-band exciton, trion, and *H*-band features clearly suggests that many particle interactions and strong electronic correlations prevail in the optical spectra of SWNTs even in the heavily doped regime with $\approx$1 h·nm^{-1}.

CONCLUSIONS

In conclusion, we have studied the effect of gate doping on the optical spectra and electronic correlations in (6,5) s-SWNTs. We showed that a quantitative analysis of gate-induced doping is ideally carried out using the oscillator strength of the first sub-band exciton. In contrast, PL intensities were shown to depend nonlinearly on free-carrier densities and thus systematically yield smaller fundamental band gaps. We discussed a simple model which describes changes of carrier densities due to gate doping in the presence of strong electronic correlations. The model predicts that gate doping of 1D semiconductors is initiated at the band edge of the undoped system by a stepwise increase of the carrier density by $32m_{eff}b/(\pi^2\hbar^2)$, which is accompanied by a band shift $\Delta\epsilon = 32m_{eff}b^2/\pi^2\hbar^2$. Spectra from hole-doped (6,5) s-SWNTs are consistent with a 40 meV upshift of the valence band edge and a charge step of 0.27 $\pm$ 0.10 h·nm^{-1}. This suggests that BGR in the heavily doped regime (n > 1 nm^{-1}) leads to at least 0.3 eV reduction of the band gap because the minority band has been predicted to shift more significantly than the majority free-carrier band.[6] For heavily doped SWNTs, the experiments also uncovered an unexpected featureless absorption band extending over the entire Pauli-blocked region (*H*-band). Interestingly, similar spectral changes have also been observed for chemically doped SWNTs,[43] suggesting a broader significance of strong electronic correlations for the optical spectra of s-SWNTs.

METHODS

s-SWNT Sample Preparation. Dispersions of (6,5)-SWNTs in toluene were prepared by sonication of 0.5 mg·mL^{-1} CoMoCAT-SWNTs (SWeNT SG 65, Southwest Nano Technologies Inc.) with 1.0 mg·mL^{-1} PFO-BPy (American Dye Source) for 7 h and subsequent benchtop centrifugation for collection of the supernatant.[33] s-SWNT films were prepared by filtration of the dispersion through cellulose acetate filter membranes (MF-Millipore VCWP, Merck Millipore). Films were subsequently

transferred to a Pt-mesh electrode or an indium-tin oxide (ITO)-covered microscope slide. The filter membrane was dissolved using an acetone bath. Spectroelectrochemical investigations of bulk suspensions of free s-SWNTs gave qualitatively and quantitatively similar results.

Electrochemical Setup. All electrochemical experiments were conducted in a 0.1 molar solution of tetrabutylammonium hexafluorophosphate (Sigma-Aldrich) in dry and degassed tetrahydrofuran under an inert argon atmosphere in a home-built spectroscopy chamber. A three-electrode setup with a platinum pseudoreference electrode, a platinum counter electrode, and different s-SWNT working electrodes was utilized. The reference was calibrated *versus* decamethylferrocene (Sigma-Aldrich), leading to a value of 280 $\pm$ 40 mV *vs* SHE. An EG&G model 363 potentiostat was used for potentiostatic control.

UV−vis−NIR Absorption Measurements. Absorption measurements under potentiostatic control were carried out with a Cary-5000 UV−vis−NIR absorption spectrometer, using the described electrochemical setup with an s-SWNT film on a Pt-mesh as the working electrode. Spectra were recorded for each potential step after allowing for a settling time of 2 min.

Simultaneous Absorption and Photoluminescence Measurements. These were obtained with a home-built optical setup using an ITO-covered microscope slide as the working electrode onto which the s-SWNTs were placed. The light source for absorption measurements and PL excitation was a SuperK EXTREME EXR-15 (NKT Photonics) in combination with various band-pass and OD filters (Thorlabs). For signal detection, a Shamrock 303i spectrometer with InGaAs line array (iDus DU491A, Andor) was utilized. Spectra were recorded for each potential step after allowing for a settling time of 1 min.

Global Data Analysis. This was performed by a least-squares fitting routine written for IGOR Pro 6.3 (WaveMetrics). Absorption spectra, presented as ($n \times m$) data matrices with n elements in wavelength and m elements in potential dimension, were modeled by multiplying a ($n \times q$) spectral matrix and a ($q \times m$) weight matrix, with q being the number of individual components, thus directly yielding the components' spectra and weight progressions as fit results.[38] Three spectral components were sufficient to describe the data, both in the NIR and the vis spectral regions. Additional components did not lead to a significant improvement of spectral fits. Final optimization of the fit was performed by constraining the third components spectra in the ($n \times q$) matrices to the experimentally recorded spectra at the highest gate potential. The weight parameters in the ($q \times m$) matrices were set to 1, 0, and 0 at the lowest potential for the first, second, and third component, respectively.

Conflict of Interest: The authors declare no competing financial interest.

Acknowledgment. T.H. acknowledges financial support by the DFG through INST 93/756-1. F.S. acknowledges discussions on global analysis with Larry Luer. T.H. acknowledges many stimulating discussions with Richard Martel.

Supporting Information Available: The Supporting Information is available free of charge on the ACS Publications website at DOI: 10.1021/acsnano.5b04707.

Additional experimental details and figures (PDF)

REFERENCES AND NOTES

1. Mahan, G. D. *Many-Particle Physics*; Kluwer Academic: New York, 2000.
2. Haug, H.; Koch, S. W. *Quantum Theory of the Optical and Electronic Properties of Semiconductors*; World Scientific: Singapore, 1994.
3. Wang, F.; Dukovic, G.; Brus, L. E.; Heinz, T. F. The Optical Resonances in Carbon Nanotubes Arise From Excitons. *Science* **2005**, *308*, 838–841.
4. Maultzsch, J.; Pomraenke, R.; Reich, S.; Chang, E.; Prezzi, D.; Ruini, A.; Molinari, E.; Strano, M. S.; Thomsen, C.; Lienau, C. Exciton Binding Energies in Carbon Nanotubes from Two-Photon Photoluminescence. *Phys. Rev. B: Condens. Matter Mater. Phys.* **2005**, *72*, 241402.
5. Lefebvre, J.; Finnie, P. Excited Excitonic States in Single-Walled Carbon Nanotubes. *Nano Lett.* **2008**, *8*, 1890–1895.
6. Spataru, C. D.; Léonard, F. Tunable Band Gaps and Excitons in Doped Semiconducting Carbon Nanotubes Made Possible by Acoustic Plasmons. *Phys. Rev. Lett.* **2010**, *104*, 177402.
7. Deslippe, J.; Dipoppa, M.; Prendergast, D.; Moutinho, M. V. O.; Capaz, R. B.; Louie, S. G. Electron-Hole Interaction in Carbon Nanotubes: Novel Screening and Exciton Excitation Spectra. *Nano Lett.* **2009**, *9*, 1330–1334.
8. Matsunaga, R.; Matsuda, K.; Kanemitsu, Y. Observation of Charged Excitons in Hole- Doped Carbon Nanotubes Using Photoluminescence and Absorption Spectroscopy. *Phys. Rev. Lett.* **2011**, *106*, 037404.
9. Santos, S. M.; Yuma, B.; Berciaud, S.; Shaver, J.; Gallart, M.; Gilliot, P.; Cognet, L.; Lounis, B. All-Optical Trion Generation in Single-Walled Carbon Nanotubes. *Phys. Rev. Lett.* **2011**, *107*, 187401.
10. Heller, I.; Kong, J.; Heering, H. A.; Williams, K. A.; Lemay, S. G.; Dekker, C. Individual Single-Walled Carbon Nanotubes as Nanoelectrodes for Electrochemistry. *Nano Lett.* **2005**, *5*, 137–142.
11. Heller, I.; Kong, J.; Williams, K. A.; Dekker, C.; Lemay, S. G. Electrochemistry at Single- Walled Carbon Nanotubes: The Role of Band Structure and Quantum Capacitance. *J. Am. Chem. Soc.* **2006**, *128*, 7353–7359.
12. Sgobba, V.; Guldi, D. M. Carbon Nanotubes-Electronic/Electrochemical Properties and Application for Nanoelectronics and Photonics. *Chem. Soc. Rev.* **2009**, *38*, 165–184.
13. Frank, O.; Kavan, L.; Green, A. A.; Hersam, M. C.; Dunsch, L. *In-Situ* Vis/NIR Spectroelectrochemistry of Single-Walled Carbon Nanotubes Enriched With (6,5) Tubes. *Phys. Status Solidi B* **2008**, *245*, 2239–2242.
14. Kalbac, M.; Kavan, L.; Dunsch, L. Changes in the Electronic States of Single-Walled Carbon Nanotubes as Followed by a Raman Spectroelectrochemical Analysis of the Radial Breathing Mode. *J. Phys. Chem. C* **2008**, *112*, 16759–16763.
15. Kavan, L.; Frank, O.; Green, A. A.; Hersam, M. C.; Koltai, J.; Zólyomi, V.; Kürti, J.; Dunsch, L. *In Situ* Raman Spectroelectrochemistry of Single-Walled Carbon Nanotubes: Investigation of Materials Enriched with (6,5) Tubes. *J. Phys. Chem. C* **2008**, *112*, 14179–14187.
16. Paolucci, D.; Franco, M. M.; Iurlo, M.; Marcaccio, M.; Prato, M.; Zerbetto, F.; Pénicaud, A.; Paolucci, F. Singling out the Electrochemistry of Individual Single-Walled Carbon Nanotubes in Solution. *J. Am. Chem. Soc.* **2008**, *130*, 7393–7399.
17. Rafailov, P. M.; Thomsen, C.; Dettlaff-Weglikowska, U.; Roth, S. High Levels of Electrochemical Doping of Carbon Nanotubes: Evidence for a Transition from Double-Layer Charging to Intercalation and Functionalization. *J. Phys. Chem. B* **2008**, *112*, 5368–5373.
18. Zukalova, M.; Tarabek, J.; Kalbac, M.; Kavan, L.; Dunsch, L. *In Situ* Optical Spectroelectrochemistry of Single-Walled Carbon Nanotube Thin Films. *J. Solid State Electrochem.* **2008**, *12*, 1279–1284.
19. Kalbac, M.; Farhat, H.; Kavan, L.; Kong, J.; Sasaki, K.-I.; Saito, R.; Dresselhaus, M. S. Electrochemical Charging of Individual Single-Walled Carbon Nanotubes. *ACS Nano* **2009**, *3*, 2320–2328.
20. Tanaka, Y.; Hirana, Y.; Niidome, Y.; Kato, K.; Saito, S.; Nakashima, N. Experimentally Determined Redox Potentials of Individual (n,m) Single-Walled Carbon Nanotubes. *Angew. Chem., Int. Ed.* **2009**, *48*, 7655–7659.
21. Kavan, L.; Rapta, P.; Dunsch, L. *In Situ* Raman and Vis-NIR Spectroelectrochemistry at Single-Walled Carbon Nanotubes. *Chem. Phys. Lett.* **2000**, *328*, 363–368.
22. Kavan, L.; Rapta, P.; Dunsch, L.; Bronikowski, M. J.; Willis, P.; Smalley, R. E. Electrochemical Tuning of Electronic Structure of Single-Walled Carbon Nanotubes: *In-Situ* Raman and Vis-NIR Study. *J. Phys. Chem. B* **2001**, *105*, 10764–10771.
23. Hirana, Y.; Tanaka, Y.; Niidome, Y.; Nakashima, N. Strong Micro-Dielectric Environment Effect on the Band Gaps of

(n,m) Single-Walled Carbon Nanotubes. *J. Am. Chem. Soc.* **2010**, *132*, 13072–13077.
24. Dragin, F.; Pénicaud, A.; Iurlo, M.; Marcaccio, M.; Paolucci, F.; Anglaret, E.; Martel, R. Raman Doping Profiles of Polyelectrolyte SWNTs in Solution. *ACS Nano* **2011**, *5*, 9892–9897.
25. Kavan, L.; Dunsch, L. Spectroelectrochemistry of Carbon Nanotubes. *ChemPhysChem* **2011**, *12*, 47–55.
26. Hong, L.; Toshimitsu, F.; Niidome, Y.; Nakashima, N. Microenvironment Effect on the Electronic Potentials of Individual (6,5) Single-Walled Carbon Nanotubes. *J. Mater. Chem. C* **2014**, *2*, 5223.
27. Hong, L.; Toshimitsu, F.; Niidome, Y.; Nakashima, N. Redox Properties of a Single (7,5) Single-Walled Carbon Nanotube Determined By an *In Situ* Photoluminescence Spectroelectrochemical Method. *Nanoscale* **2014**, *6*, 12798.
28. Schäfer, S.; Cogan, N. M. B.; Krauss, T. D. Spectroscopic Investigation of Electrochemically Charged Individual (6,5) Single-Walled Carbon Nanotubes. *Nano Lett.* **2014**, *14*, 3138–3144.
29. Deria, P.; Olivier, J.-H.; Park, J.; Therien, M. J. Potentiometric, Electronic, and Transient Absorptive Spectroscopic Properties of Oxidized Single-Walled Carbon Nanotubes Helically Wrapped by Ionic, Semiconducting Polymers in Aqueous and Organic Media. *J. Am. Chem. Soc.* **2014**, *136*, 14193–14199.
30. Ilani, S.; Donev, L. A. K.; Kindermann, M.; McEuen, P. L. Measurement of the Quantum Capacitance of Interacting Electrons in Carbon Nanotubes. *Nat. Phys.* **2006**, *2*, 687–691.
31. Perebeinos, V.; Tersoff, J.; Avouris, P. Electron-Phonon Interaction and Transport in Semiconducting Carbon Nanotubes. *Phys. Rev. Lett.* **2005**, *94*, 086802.
32. Murakami, Y.; Lu, B.; Kazaoui, S.; Minami, N.; Okubo, T.; Maruyama, S. Photoluminescence Sidebands of Carbon Nanotubes Below the Bright Singlet Excitonic Levels. *Phys. Rev. B: Condens. Matter Mater. Phys.* **2009**, *79*, 195407.
33. Ozawa, H.; Ide, N.; Fujigaya, T.; Niidome, Y.; Nakashima, N. One-pot Separation of Highly Enriched (6,5)-Single-walled Carbon Nanotubes Using a Fluorene-based Copolymer. *Chem. Lett.* **2011**, *40*, 239–241.
34. Luer, L.; Hoseinkhani, S.; Polli, D.; Crochet, J.; Hertel, T.; Lanzani, G. Size and Mobility of Excitons in (6,5) Carbon Nanotubes. *Nat. Phys.* **2009**, *5*, 54–58.
35. Miyauchi, Y.; Ajiki, H.; Maruyama, S. Electron-Hole Asymmetry in Single-Walled Carbon Nanotubes Probed by Direct Observation of Transverse Quasidark Excitons. *Phys. Rev. B: Condens. Matter Mater. Phys.* **2010**, *81*, 121415.
36. Cognet, L.; Tsyboulski, D. A.; Rocha, J.-D. R.; Doyle, C. D.; Tour, J. M.; Weisman, R. B. Stepwise Quenching of Exciton Fluorescence in Carbon Nanotubes by Single-Molecule Reactions. *Science* **2007**, *316*, 1465–1468.
37. Hertel, T.; Himmelein, S.; Ackermann, T.; Stich, D.; Crochet, J. Diffusion Limited Photoluminescence Quantum Yields in 1-D Semiconductors: Single-Wall Carbon Nanotubes. *ACS Nano* **2010**, *4*, 7161–7168.
38. Henry, E. R. The Use of Matrix Methods in the Modeling of Spectroscopic Data Sets. *Biophys. J.* **1997**, *72*, 652–673.
39. Spataru, C. D.; Léonard, F. Quasiparticle and Exciton Renormalization Effects in Electrostatically Doped Semiconducting Carbon Nanotubes. *Chem. Phys.* **2013**, *413*, 81–88.
40. Schoppler, F.; Mann, C.; Hain, T. C.; Neubauer, F. M.; Privitera, G.; Bonaccorso, F.; Chu, D. P.; Ferrari, A. C.; Hertel, T. Molar Extinction Coeffcient of Single-Wall Carbon Nanotubes. *J. Phys. Chem. C* **2011**, *115*, 14682–14686.
41. Mak, K. F.; Ju, L.; Wang, F.; Heinz, T. F. Optical Spectroscopy of Graphene: From the Far Infrared to the Ultraviolet. *Solid State Commun.* **2012**, *152*, 1341–1349.
42. Hagen, A.; Hertel, T. Quantitative Analysis of Optical Spectra from Individual Single- Wall Carbon Nanotubes. *Nano Lett.* **2003**, *3*, 383–388.
43. Zheng, M.; Diner, B. A. Solution Redox Chemistry of Carbon Nanotubes. *J. Am. Chem. Soc.* **2004**, *126*, 15490–15494.